CHAPTER 4

4.1 Introduction

In order to explore novel physical properties and phenomena and realize potential applications of nanostructures and nanomaterials in various fields, the synthesis of nanoparticles is the first and foremost step followed by characterization of nanomaterials with the help of sophisticated analytical techniques. The removal of pollutants by adsorption technique is influenced markedly by the nature of the adsorbate and the adsorbent employed for the purpose. It has profound effects on both the rate and the capacity of the removal. Since the nature of adsorption is largely dependent on the adsorbate species and the constituents of the adsorbents, it become requisite to characterize them to ensure a better insight of the mechanism of adsorption of pollutants. This chapter embodies information regarding synthesis and characterization of nanomaterials used as adsorbents for metal removal from aqueous solutions.

4.2 Synthesis of nano-alumina (n-Al_2O_3)

4.2.1 Experimental set-up for synthesis of nano-alumina

Alumina nano-particles were synthesized according to the sol-gel method, with minor modifications [Dubey et al., 2016]. For the synthesis, 0.5 M $Al_2SO_4.16H_2O$ (A) and 0.2 M CTAB (B) solutions were prepared separately using distilled water. Both the solutions (A+B) were then gradually mixed with continuous magnetic stirring. Afterwards, the above

solution mixture was precipitated through 25% ammonium hydroxide solution with gradual magnetic stirring. A white gel of aluminum hydroxide was formed due to precipitation reaction which was then dried into a hot air oven at 75ºC. The air dried solid mass was then crushed and ground in agate mortar-pestle to get particles of uniform size. Thereafter, the powdered material was calcined in a muffle furnace at 1000ºC for 2 h to get final aluminum oxide nano-particles which was again ground, sieved through a sieve and stored for characterization and experimentation purposes.

4.2.3 Characterization of synthesized nano-alumina

4.2.3.1 X-Ray diffraction analysis

Phase purity and identification of the synthesized nano-adsorbent was accomplished by means of X-ray diffractrometry in the 2θ range of 10º to 80º with scan rate of 3deg/min. The characteristic intense peaks corresponding to (111), (220), (311), (222), (400), (511) and (440) planes Figure 4.1, confirmed the formation of γ-phase of alumina nanoparticles which was in accord to the (JCPDS card No. 10-0425). No other peak except n-Al_2O_3 in the XRD pattern confirms the purity of synthesized material.

The average crystallite size of the material was calculated by using the Scherrer's formula [Scherrer, 1981]:

$$\text{Crystallite size} = K\lambda / \beta \cos\theta \qquad (4.1)$$

Here K is shape factor; λ, β and θ corresponds to the X-ray wavelength (A^0), the full width at half maximum (FWHM) of the diffraction peak and the Bragg diffraction angle

(rad.) respectively. The calculated crystallite size was found to vary from 3-6 nm. There are no other peaks of impurities other than the desired material are seen in the diffraction pattern of alumina nanoparticles which suggests the phase purity of the synthesized nanomaterial. Further, it was reported that calcination temperature upto 1000ºC leads to the formation of γ-phase of Al_2O_3 which is based on a distorted spinel structure, due to progressive dehydration and desorption of surface hydroxyl groups [Cava et al., 2007].

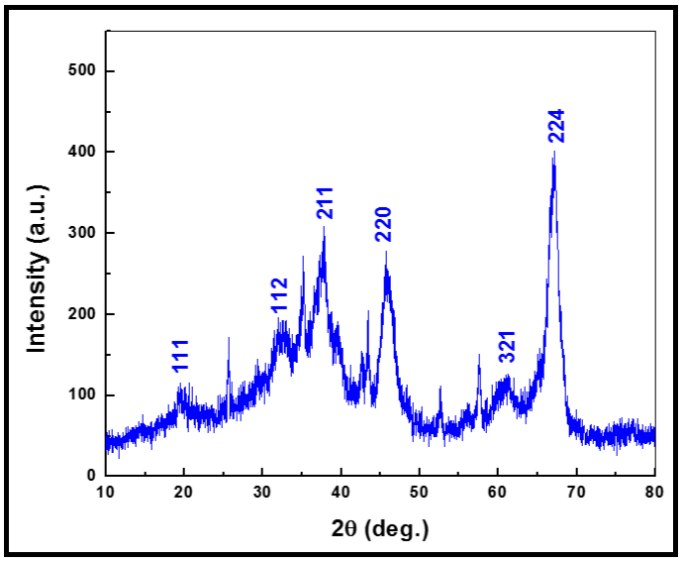

Figure 4.1 X-ray diffraction (XRD) pattern of nano-alumina

4.2.3.2 Fourier transform infra-red analysis

The FTIR spectrum of the pure alumina was recorded for illustration of surface functional groups (Figure 4.2). The presence of peak in the region 3000 to 3600 cm^{-1} is related to the lattice water molecules which indicate the presence of moisture in the powder or KBr pellet. In the alumina, the vibrations of the OH, Al-OH, and Al-O bonds

generated the observed bands in the infrared region. The stretching vibration of the OH ions of residual water and solvent in the gel produced a very intense broad band at 3451 cm^{-1}, whereas their bending vibration generated the band at 1636 cm^{-1}. The stretching vibrations of the Al-OH bond gave rise to the band at 1555 cm^{-1}.

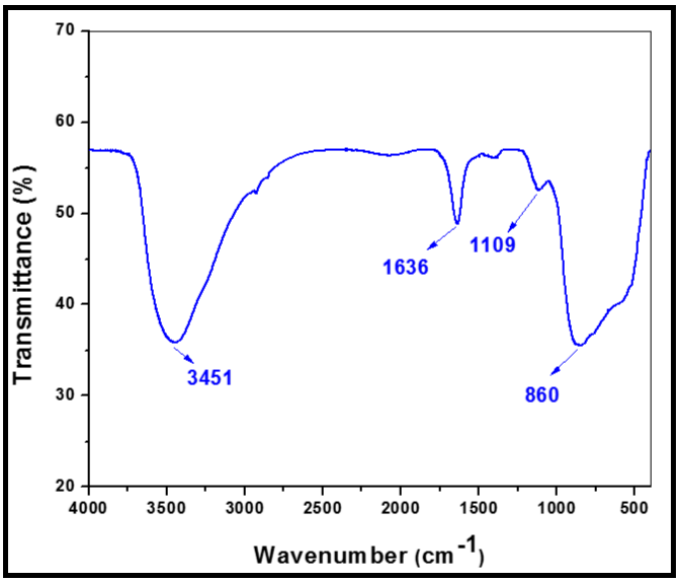

Figure 4.2 Fourier transform infra-red (FTIR) spectrum of nano-alumina

The weak bands observed at 1109 cm^{-1} was produced by Al-O bonds [Sharma et al. 2010]. The presence of all these peaks ensured the formation of alumina nanoparticles.

4.2.3.3 Electron microscopic analysis

For topographical aspect and particle size of the synthesized alumina nanoparticles electron microscopic (TEM and SEM) analysis was carried out. TEM micrograph (Figure 4.3 A) displays the formation of aggregates of particles which is

probably due to small size of nanoparticles. The average particle size was estimated to vary from 3-12 nm which might be due to the addition of CTAB as surfactant that helped in the reduction of particle size. Its corresponding SAED pattern is also presented here which shows various planes corresponding to the planes present in X-ray diffractogram (Figure 4.3 B).

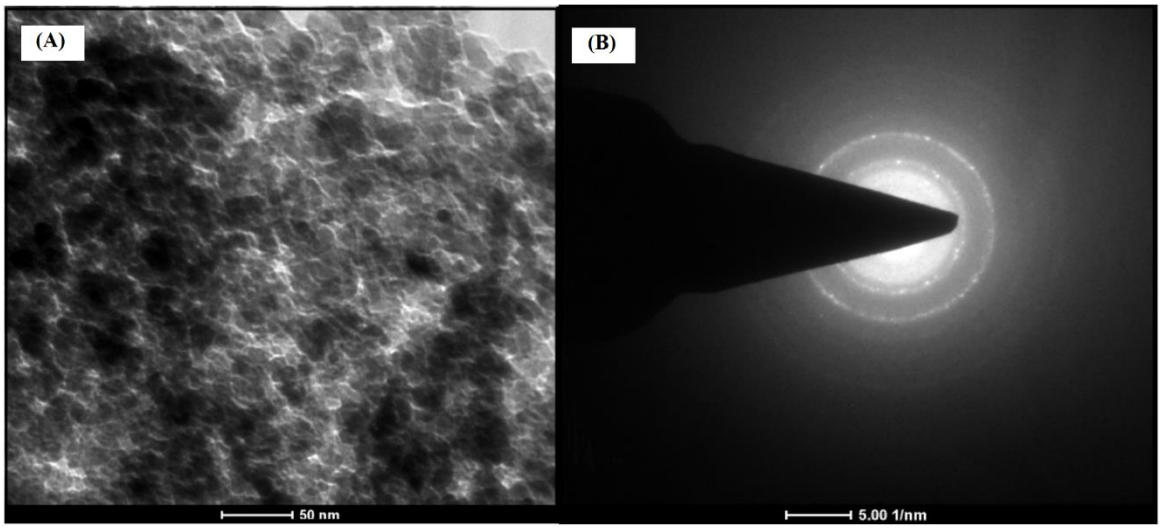

Figure 4.3 (A) Transmission electron micrograph; and (B) Selected area electron diffraction (SAED) pattern of nano-alumina

The surface of the nano-alumina was found to be spherical as evident from SEM micrograph (Figure 4.4) which was unforeseeable from micrograph obtained through Transmission electron microscope.

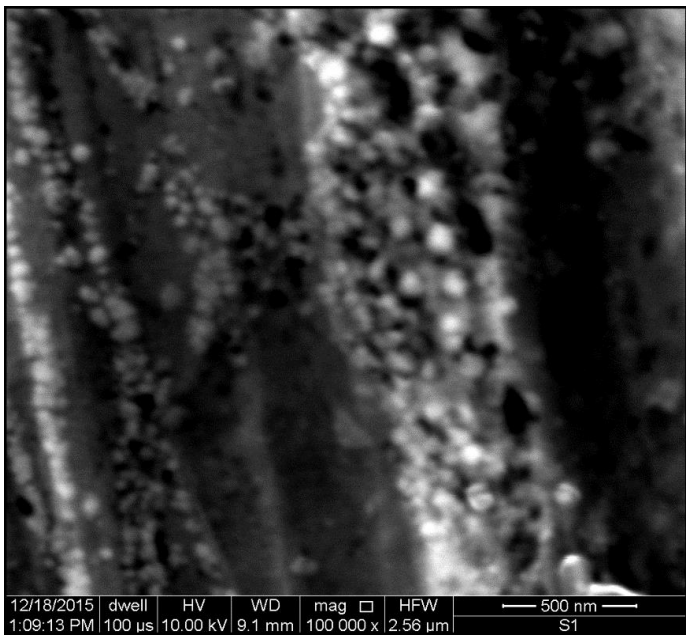

Figure 4.4 Scanning electron micrograph (SEM) of nano-alumina

EDX analysis was performed to determine the elemental constituents of pure alumina nanoparticles. From the EDX pattern (Figure 4.5) it can be clearly seen that peaks of only Al and O are present indicating the high-phase purity of the synthesized material.

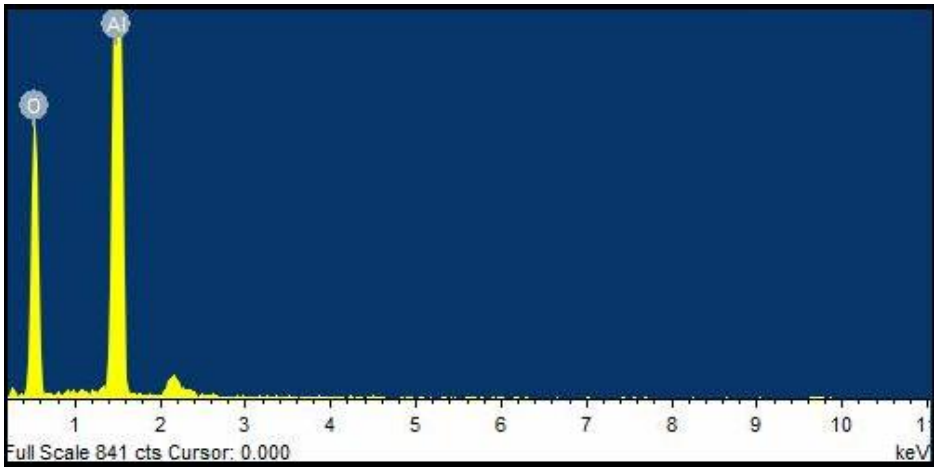

Figure 4.5 Energy dispersive x-ray (EDAX) pattern of nano-alumina

The surface area of the alumina nanoparticles was estimated as 58.49 m^2/g.

4.3 Synthesis of nano-Cupric oxide (n-CuO)

4.3.1 Green synthesis

During nanoparticle synthesis and stabilization, chemicals used are toxic and lead to formation of some non-eco-friendly by-products. Green synthesis involves the use of environmentally benign materials that offers numerous benefits in terms of eco-friendliness and compatibility as it does not involve any toxic material during synthesis protocol. Therefore, several green approaches have been adopted to minimize the use of certain chemicals utilized during nanoparticle synthesis [Kanipandian and Thirumurugan, 2014; Muthukrishnan et al., 2015]. The plant *Calotropis procera* belonging to the family Asclepiadaceae, also called as Alarka, Mandara, Shwetarka, Vasuka, is a xerophytic shrub distributed throughout India. The different parts of the plant are known to be used in Indian traditional medicine for the treatment of painful muscular spasm, dysentery, fever, rheumatism, asthma and as an expectorant and purgative. The chemical composition of crude latex shows that more than 80% of its dry mass corresponds to the rubber and remaining 20% contains various soluble biologically active compounds rich in carbohydrates, proteins, amino acids, vitamins, lipids, anti-oxidants enzymes, tryptophan, alkaloids, resins, and tannins, etc [Das and Sharma, 2011]. Furthermore, it is known to have predominantly the alkaloids namely calotropin, calactin, and calotoxin [Singh et al., 2011]. However, its main constituent is reported to be rubber, which is highly insoluble in water [Silva et al., 2010].

4.3.2. Experimental set up for synthesis of CuO nanoparticles

For the synthesis of CuO nanoparticles, simple precipitation method was adopted. Metal precursors of different molar concentration were prepared and precipitated with the precipitating agent. Afterwards, precipitate was washed, dried and calcined at various temperatures. On the basis of findings of several characterizations of these materials, the one with the best response was selected for the study.

Precursor solutions were prepared by dissolving appropriate amounts of $CuSO_4.5H_2O$ and NaOH separately. Thereafter, a known amount of latex obtained from *Calotropis procera* plant was added into the 0.2 M Cu^{2+} solution with stirring for approximately 10 min. Precipitation was achieved at room temperature by adding 0.5 M NaOH to the above mixture by continuous stirring on a magnetic stirrer. After completion of precipitation reaction, green coloured precipitate was separated by centrifugation at 10000 rpm for 10 min. Thereafter, greenish precipitate was repeatedly washed with distilled water to remove any impurity adhered on the surface and finally washed with ethyl alcohol for the removal of any unreacted particle. After proper multistep washing, nanoparticles were dried in hot air oven at 70^0C for 24h. Later on, dried green powder of $Cu(OH)_2$ was crushed in agate mortar pestle, sieved and calcined at 600ºC for 2 h with heating rate of 10ºC/min. On calcination, green colour of precipitate transformed into black coloured cupric oxide particles.

4.3.3 Characterization of synthesized nano-cupric oxide

4.3.3.1 X-Ray diffraction analysis

The purity and phase of the powdered CuO was determined by X-ray diffraction (XRD) technique employing Cu Kα radiation (1.542 Aº) in the 2θ range of 20-80º at a step rate of 0.4 $\theta s^{-1}$and the typical diffraction pattern has been depicted in Figure 4.6. The diffractrogram revealed that all the peaks in the range of $20^0 < 2\theta < 80^0$ were well indexed to monoclinic symmetry of copper oxide nanostructures consistent with JCPDS (Joint Committee on Powder Diffraction Standards) file no. 80-1916. The peak positions and relative intensities confirmed the formation of the synthesized material as CuO nanoparticles. No other peaks characteristics of other impurities such as $Cu(OH)_2$ and Cu_2O were detected indicating the single-phase high purity of the final product. The average size of the nanomaterial was estimated as 28 nm by using the Scherrer's formula (Eq. 3.1).

4.3.3.2 Fourier transform infra-red analysis

FT-IR spectra of CuO nanoparticles (Figure 4.7) showed obvious absorption peaks at around 519 and 598 cm^{-1} which were assigned to vibrations of Cu-O bands (Guedes et al. 2009). The absorption band at about 3432 cm^{-1} resulted due to the vibration mode of the absorbed water. No infrared active modes from Cu_2O were detected in the spectrum suggested the result to be in consistent with the XRD results.

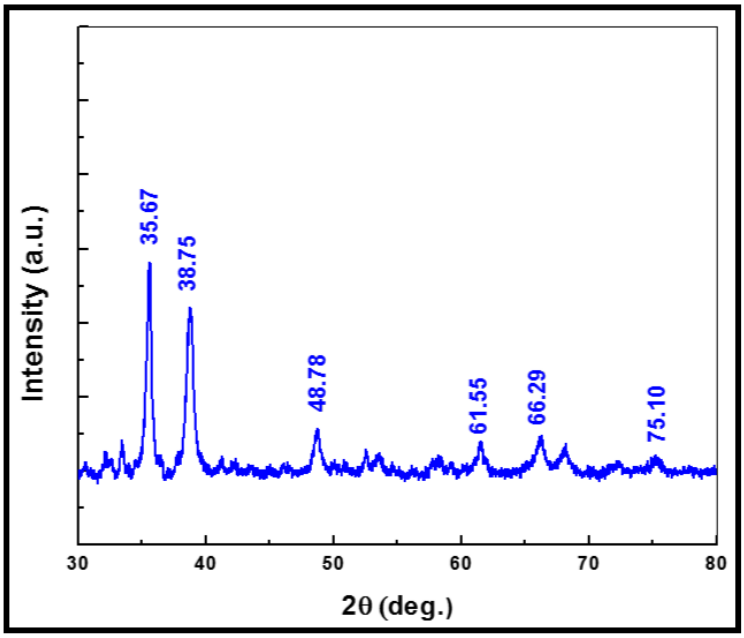

Figure 4.6 X-ray diffraction pattern (XRD) pattern of nano-cupric oxide

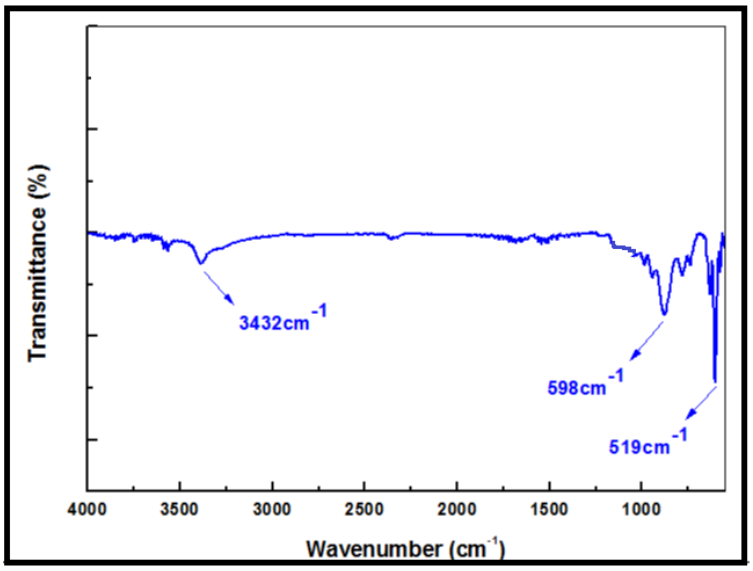

Figure 4.7 Fourier transform infra-red (FTIR) spectrum of nano-cupric oxide

4.3.3.3 Electron microscopic analysis

Electron misroscopic analysis was performed for determination of grain size, morphology and structure of CuO nanoparticles. TEM analysis revealed the particles were grown quasi-spherical in shape with slight agglomeration but in nanometer range (Figure 4.8).

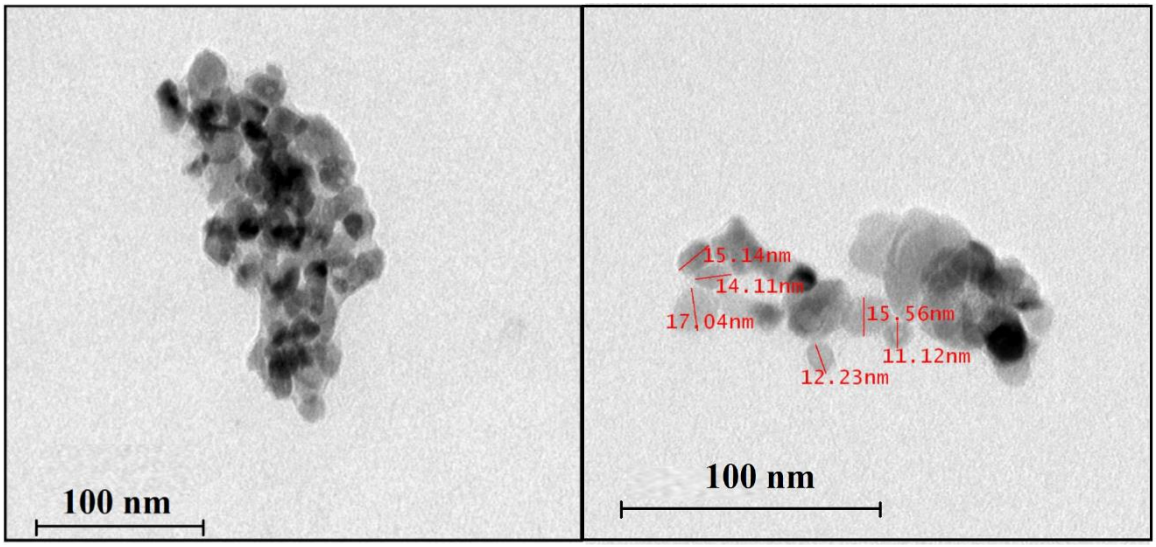

Figure 4.8 Transmission electron micrograph (TEM) of nano-cupric oxide

The information regarding surface morphology was provided by SEM analysis that depicted the surface of CuO nanoparticles was somewhat rough in nature and have dimensions in nano-meter range (Figure 4.9). Probably, the constituents present in the latex used for stabilization of the particles assisted in the reduction of particle size and thus resulted in the formation of dispersed CuO nanoparticles.

For further demonstration, EDAX was performed for the CuO nanoparticles and the EDAX spectrum as shown in Figure 4.10 evidenced the presence of Cu and O as the only elementary components.

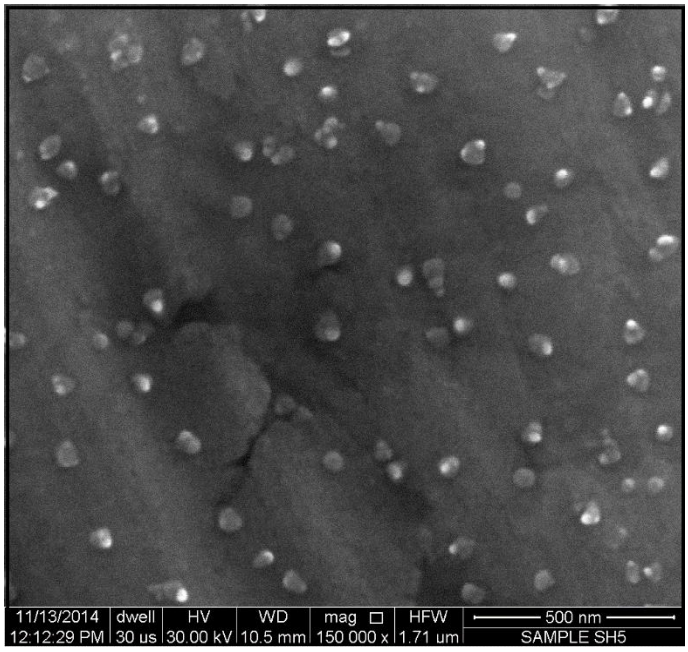

Figure 4.9 Scanning electron micrograph (SEM) of nano-cupric oxide

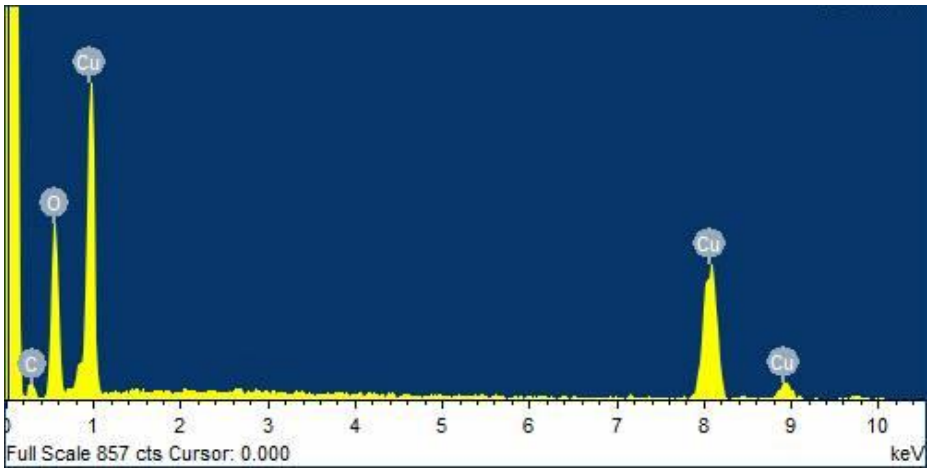

Figure 4.10 Energy dispersive x-ray (EDAX) pattern of nano-cupric oxide

The surface area of the cupric oxide nanoparticles was estimated as 20 m^2/g.

4.4 Determination of point of zero charge (pH_{zpc})

pH_{zpc} of n-Al_2O_3 was also determined by reported method. For its determination, 0.20 g of n-Al_2O_3 was added in to 50 mL of 0.01 M NaCl solution having different pH range from 2 to 12 and this solution was kept for 48 h. After preset time, adsorbent was separated from NaCl solution and final pH of NaCl solution was measured [Yadav et al., 2012]. A graph was plotted between initial and final pH of NaCl solution and the point of intersection of 'pH_{final} vs. $pH_{initial}$' curves was recorded as pHzpc of the n-Al_2O_3.

The pH_{zpc} of n-Al_2O_3 was recorded as 4.0 (Figure 4.11) and for n-CuO, it was found to be 6.0 (Figure 4.12).

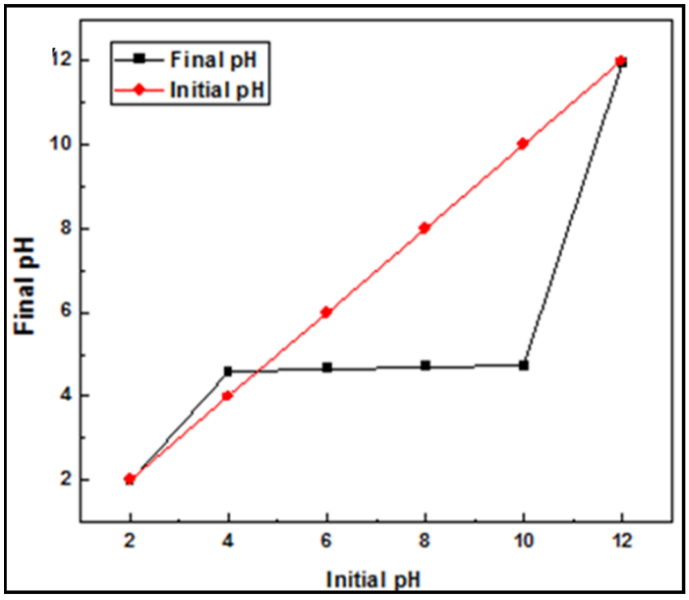

Figure 4.11 pHzpc of synthesized nano-alumina

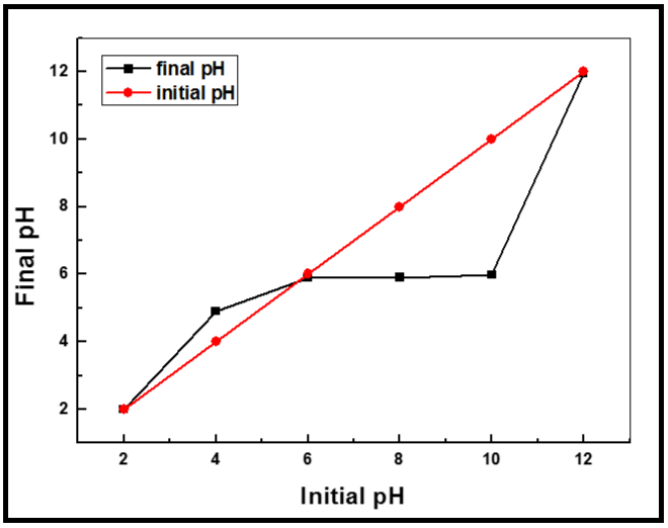

Figure 4.12 pHzpc of synthesized nano-cupric oxide